Modelling the hydromechanical response in the vicinity of the Koyna reservoir (India): results for the initial filling period

Pierre Gavrilenko, Chandramani Singh, R. Chadha

Geophysical Journal International

Geophys. J. Int. (2010) **183,** 461–477 doi: 10.1111/j.1365-246X.2010.04752.x

Modelling the hydromechanical response in the vicinity of the Koyna reservoir (India): results for the initial filling period

P. Gavrilenko,[1] Chandrani Singh[2] and R. K. Chadha[2]

[1] *Geosciences Rennes, UPR* 4661, *CNRS Campus Beaulieu, Bat.*15, *Avenue du G*^{al} *Leclerc,* F35042 *Rennes Cedex, France. E-mail: Pierre.Gavrilenko@univ-rennes1.fr*

[2] *National Geophysical Research Institute, Council of Scientific and Industrial Research, Uppal Road, Hyderabad* 500 007, *India*

Accepted 2010 July 26. Received 2010 July 23; in original form 2009 July 23

SUMMARY

The seismic activity in the Koyna area is clearly related to the water impoundment of the Koyna dam in 1962, and has reached a remarkable level with the occurrence of a major event of magnitude 6.3 in 1967 December 10. We present a homogeneous poroelastic model based on analysis of the first eight years of seismicity, which aims to link the water-level fluctuations of the reservoir with the seismicity. Starting from a discretized lake, we calculate the stress field resulting from the water-level fluctuations and the pore pressure changes due to the undrained and the diffusive responses of the medium. Then, we compare the Coulomb stress variations with a set of relocated seismic events. We find that more than 80 per cent of the relocated events before the M6.3 event are well described by this poroelastic model, leading us to derive a suitable diffusivity $c_p = 0.2\,\mathrm{m}^2\,\mathrm{s}^{-1}$. Then, we model the response of the system after the M6.3 event of 1967 December 10, by comparing the variation of the Coulomb stress field with the spatio-temporal characteristics of the relocated post-seismic events and the decay of aftershocks with time. We find that compared to before the main event a tenfold increase in hydraulic diffusivity is required to satisfactorily describe the aftershock decay with the appropriate Omori exponent. Although this increase in diffusivity may be physically related to the main shock we also note that events later than 9 months after the main shock are not well explained. We therefore propose an alternative hydrological model, which involves two compartments of contrasting diffusivities.

Key words: Hydrogeophysics; Permeability and porosity; Earthquake interaction, forecasting and prediction.

1 INTRODUCTION

1.1 Presentation of the seismicity in Koyna area and of previous analyzes

Over the last 45 yr, the prevailing seismicity with $M > 5.0$ has led to a great scientific and practical interest in studying Reservoir Triggered Seismicity (RTS) in the Koyna–Warna region. The area is located to the east of the Western Ghats of the South Indian Shield (Fig. 1a). Prior to the construction of the Koyna dam in 1962, the region did not have any historical record of earthquake activity over at least the preceding 100 yr (Verma 1985). The first seismological observatory consisting of four stations was established by the Maharashtra Engineering Research Institute (MERI) in 1963 to monitor the continuous seismic activity in the Koyna region (Talwani 1997a). Frequent microearthquakes were recorded soon after the filling of the reservoir, which culminated in an earthquake of magnitude 6.3 in 1967 December 10, which is known as the ever largest RTS (in the following, we refer to this date as t_E). Our study covers the first 8 yr of the existence of the reservoir up to 20 months after t_E, ranging from May 1961 up to the middle of 1969. Talwani (1997a) relocated 64 events that occurred from 1963 to t_E using revised location parameters. (See Table A1 in Appendix A for details of epicentral characteristics of the events and their magnitudes). It was observed that most of the earthquakes during this period are located north of the East–West reach of the Koyna River. Using relocated events, Talwani (1997a) shows that, after t_E, most of the earthquakes seem to be located to the south of the previous events. A total of 26 events were relocated from t_E up to the middle of 1969 (Table A2 in Appendix A). Fig. 1(a) reports the epicentre locations of all these events.

The geological setting of the region is characterized by the Deccan Traps, dated at 67.4 Ma (Duncan & Pyle 1988), which comprise several sequences of lava flows. Although these massive compact lava sequences have low permeability, there is significant migration of water through faults, fractures, columnar jointing and vesicles. The area is criss-crossed by several steeply dipping fractures, faults and lineaments. The seismicity is bounded to the west by the Koyna

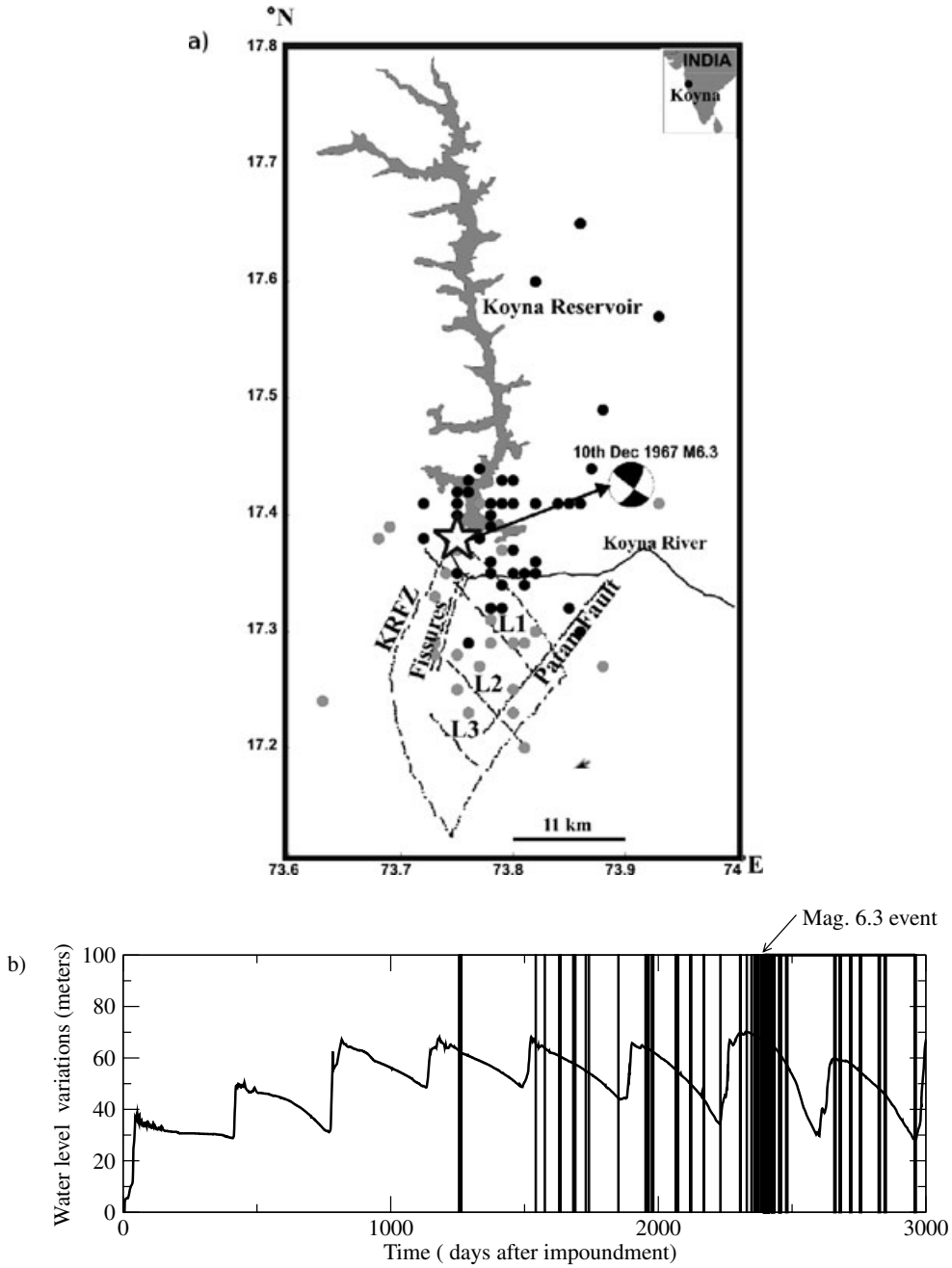

Figure 1. (a) Map showing location of Koyna reservoir in Western India, along with the inferred fault in the region. L1, L2 and L3 are the transverse faults/lineaments, and two major NE–SW trending fault zones corresponding to the KRFZ and the Patan Fault. The star indicates the epicentre of the largest triggered earthquake of M6.3 in 1967 December 10. The focal mechanism is given by Lee & Raleigh (1969). The zone of fissures consecutive to the M6.3 event lies to the east of the KRFZ (Talwani 1997a). (b) Record of water-level fluctuations of the reservoir. The vertical bars indicate seismic events.

River Fault Zone (KRFZ) that dips steeply to the West, and to the East by the NE–SW trending Patan Fault. The area between KRFZ and Patan Fault is intersected by a number of NW–SE fractures which may be extending down to hypocentral depths, shown here as L1, L2 and L3 (see Fig. 1a).

Gupta & Rastogi (1974) have reported a cause-and-effect relationship between water-level fluctuations in the reservoir and earthquakes in the Koyna area. The earthquake incidence is influenced by the rate of increase in water surface height, the maximum water level attained and the duration over which a high level of water is maintained. Fig. 1(b) presents the time variation of both the water level of the reservoir and the relocated seismicity over the studied period. However, we should point out that seismicity around the Koyna reservoir persists over the years, without any decrease occurring in either frequency or magnitude. This type of RTS is classified as protracted seismicity (Talwani 1997b), representing the most intriguing characteristic of seismicity in this area and the main difficulty faced by researchers. Talwani *et al.* (1996) have shown that there is a burst of seismicity in the area when the highest reservoir water level exceeds the previous maximum. This is indicative of what authors have identified as a Kaiser effect, whereby seismicity increases significantly when the applied stress overcomes the previously applied

maximum stress. Such an effect has been demonstrated by Talwani (2000), based on a set of three $M > 5$ events over a period of more than 15 yr. The $M > 5$ events seem to occur only when the water surface reaches a higher level than the previous maximum. Once this condition is fulfilled, small perturbations of fluid pressure are likely to trigger large earthquakes, indicating that the system is close to failure. On the other hand, Gupta *et al.* (2002) speculated about the persistence of seismicity in the region and pointed out the necessary but not sufficient conditions for an $M > 5.0$ earthquake to occur in the Koyna area. An earthquake may occur whenever the weekly rate of filling exceeds 12 m in the Koyna reservoir. Rajendran & Harish (2000) put forward a conceptual model based on the diffusion of reservoir water through a vertically permeable fault zone present in the area, to explain some characteristics of seismicity in the Koyna–Warna region. Their model assumes a permeable fault zone with sealed walls. The fault is thought to be continuously degenerating, which ensures the persistence of the system. However, these authors (op. cit.) acknowledged that quantitative modelling would be required to confirm their assumptions. Pandey & Chadha (2003) presented a diffusion model, assuming a highly permeable near-vertical fault zone in the basement below the Deccan traps, connected to the reservoir through fissures, fractures and vesicles in the overlying basalts.

A more general quantitative analysis of RTS has been provided by Roeloffs (1988), suggesting that the pore pressure increase causing the seismicity is related to the frequency and amplitude of lake level changes. According to Roeloffs (1988), in an homogeneous porous medium of diffusivity c_p, the fluid pressure response at depth z to a harmonic loading of amplitude P_o and pulsation ω providing a uniformly applied force to the Earth's surface, can be written as follows:

$$\frac{P(z,\omega)}{P_o} = b_1 + (1-b_1)\exp\left[-(1+i)\left(\frac{\omega}{2c_p}\right)^{1/2} z\right], \qquad (1)$$

where $b_1 = [B(1+\nu_u)][3(1-\nu_u)]^{-1}$, B is the Skempton coefficient, defined as the pore pressure change resulting from a unit change in confining pressure under undrained conditions, and ν_u the undrained counterpart of the Poisson coefficient ν of the porous material (see Rice & Cleary 1976, for details). The first term on the right-hand side of eq. (1) corresponds to the undrained part of the response. At great depth or at high frequency, the fluid pressure is equal to the static confining pressure response given by $P = b_1 P_o$. The second term represents the contribution of the diffusive pore pressure. The relative contributions of the undrained and the diffuse responses depend on the poroelastic coefficients. The amplitude and phase shift of the diffusive pressure signal also vary with the frequency of cyclic loading and depth. From eq. (1), Roeloffs (1988) derives a critical depth:

$$z_c = 2\pi\left(\frac{2c_p}{\omega}\right)^{1/2} \qquad (2)$$

below which the behaviour is fully undrained. This type of $1D$ analysis has been discussed by Talwani (1997b) in the case of Koyna. Considering annual lake-level fluctuations and larger reservoirs, deeper and more widespread zones may be reached. The initial seismicity results from the instantaneous effect of loading of the reservoir and the delayed effect due to pore pressure diffusion. The delay between initial impoundment and the larger-magnitude events may vary from months to a year depending on the availability of favourable local site conditions. Finally, Kalpna & Chander (2000) performed a quantitative analysis using a Green's functions approach. Assuming a diffusion coefficient $c_p = 10\,\mathrm{m^2\,s^{-1}}$, they show that, at 4.5 km depth, the fluid pressure response is dominated by diffusive processes. Their approach was subsequently used by Gahalaut *et al.* (2004) to determine the Coulomb stress changes due to the reservoir impoundment. These latter authors (op. cit.) indicate that the stress transfer resulting from a left lateral strike-slip fault is likely to play a role in the triggering of 'normal' earthquakes. Hence, stress interactions should also be considered in view of the persistence of seismicity in the Koyna area. Finally, in a more general discussion on the RTS topic, do Nascimento *et al.* (2005a) and do Nascimento *et al.* (2005b) have performed detailed 3-D numerical modelling of fluid diffusion in the Açu reservoir in Brazil. They show that the heterogeneous hydraulic properties of the fault system around the Açu reservoir can be inverted using the spatio-temporal distribution of RTS. Thus, according to these authors, RTS would provide a great opportunity to acquire information on large-scale fluid flow and obtain new insights on the complexity of hydraulic properties in fault zones.

1.2 Objectives

The aim of the present study is to develop a hydromechanical model to simulate the mechanical behaviour in the vicinity of Koyna lake. Even though the site has received considerable attention for about 45 yr, we still lack a comprehensive model of the coupled processes in this area. We present here an initial model based on the first eight years of existence of the system. The final objective is to model the entire hydromechanical history over more than 40 yr of functioning of the system. However, the system is becoming increasingly complex with time, since the stress field of the major events locally modifies the initial stress field. By starting modelling at the onset of reservoir filling, we can make minimal assumptions on the initial state of the medium. However, this approach has the disadvantage of leading to some specific difficulties. Seismological data are old and, as such, they do not attain the same level of confidence as in recent studies. As a consequence, we have to deal with a lack of data and sometimes poorly constrained inversions of seismological parameters. Because of this, we are obliged to perform trial and error approaches to select the parameters within the range of reported data. Our purpose here is not to boost the performance of the model artificially, but rather, by using parameters within a very reasonable range, to show that simple models can be built to describe the behaviour of the system and identify some physical mechanisms prevailing in the Koyna area. The selected models provide a first-order approach that serves as a very useful starting point for further studies based on more recent field data.

2 BACKGROUND AND METHODOLOGY

Even though we do not know the exact depth at which fluids are present in the crust or how they circulate, it is at least clear that the upper part of the crust can be treated as a porous elastic medium. As a consequence, poroelasticity is an appropriate theory to deal with fluid pressure changes in the medium. For the sake of simplicity, we consider here a uniform material so that Darcy's law applies. However, in crystalline rocks, this assumption is highly questionable, since channelizing processes may occur in relation with efficient drains. Dealing with a uniform material implies that, at spatial scales larger than the correlation length of heterogeneity, the transport properties respond as a homogeneous medium. With respect to a numerical grid, this homogenization scale should be

smaller than the grid cell spacing. However, we must bear in mind that the heterogeneities of transport properties at crustal scale are still a matter of discussion and, for instance, has led Neuman (1990) to consider embedded structures of heterogeneities. An alternative to the uniform approach would be to consider a set of discrete fractures as proposed by Talwani *et al.* (2007). However, this may lead to the introduction of additional and poorly constrained parameters into the model. To avoid dealing with these numerous parameters, we restrict ourselves to considering a uniform model in spite of the fact that it is probably an oversimplification. In the following, we assume that fluids are free to circulate down to a depth of $H =$ 12 km. To model the hydromechanical effects of reservoir filling, we need to consider the effect of loading associated with the lake-level fluctuations as well as the infiltration and diffusion of fluid below the reservoir. Although eq. (1) provides a guide to modelling these coupled effects, the present study takes into account a more complex loading, which is described in detail later. We then set the boundary and initial conditions for the numerical model and define the rules for testing it by introducing a failure criterion.

2.1 Modelling the elastic effect of water loading with time

We consider here the effect of water-level fluctuation as a result of a reservoir lake filling. As the water level rises, the weight of the water column increases and the lake extends over a wider area. This induces stress changes as well as possible water infiltration. To account for the reservoir mechanical effect in a numerical simulation, we discretize the shape of the lake using a rectangular grid and consider the water column height $h_{mn}(t - t_o)$ at each point location (x_m, y_n) in the reservoir and each value of time $t \geq t_o$, where t_o is the starting time of reservoir filling. In the following, t_o is set at zero for the sake of simplicity. The spatial distribution of fluid masses is the predominant influence as far as the elastic effects are concerned. Since the exact lake bathymetry is not known, we are forced to make some simple assumptions to derive a plausible profile for the bottom of the lake. These assumptions are based on the available data, that is the shape of the lakeshore, the total volume of the reservoir, the water level measured close to the dam, denoted as $h(t)$, and the gradient of the river stream flowing at the bottom of the lake. In Appendix B, we present the procedure followed to derive the bathymetric profile shown in Fig. 2. In this figure, the gradient of the river stream flowing at the bottom of the lake is $\gamma = 1.0$ m km^{-1}, in agreement with the longitudinal river profile shown in fig. 4 of Naik *et al.* (2001). The modelling depends on the assumption that the river stream flows in the middle of the lake and that the bottom of the lake rises from the river bed up to the lakeshore. This last assumption cannot be relaxed because it ensures consistency between the available data. Although some slight deviations are likely compared with the real lake bathymetry, the main features of the mass distribution are taken into account.

Let us consider the water level $h(t)$ at time t. The column of water at (x_m, y_n) can be expressed as:

$$h_{m,n}(t) = [h(t) - D_{m,n}] \times H_e[h(t) - D_{m,n}], \tag{3}$$

where H_e is the Heaviside function, $D_{m,n}$ the difference of elevation between points situated at (x_m, y_n) and (x_{mo}, y_{no}), corresponding to the deepest point in the reservoir where $h(t)$ is measured. At a given time t, the loading of the surface due to a column of fluids $h_{m,n}(t)$ centred at (x_m, y_n) affects the surrounding medium and the stress field in the vicinity. Becker & Bevis (2004) have solved what they refer to as Love's problem, which concerns the surface loading applied by a uniform pressure over a rectangular region in an elastic half-space. These authors provide expressions for displacements in the three spatial dimensions everywhere in the half-space. Assuming a rectangular region centred at (x_m, y_n), the displacements at a given point (x, y, z) due to a pressure $P_{m,n}(t) = \rho_f g h_{m,n}(t)$ applied at the surface of an elastic half-space can be expressed as:

$$u_l(x, y, z, t) = P_{m,n}(t) u^o_{l[K,G;a,b]}(x - x_m, y - y_n, z), \tag{4}$$

where $1 \leq l \leq 3$ indicate the three spatial dimensions and u^o_l are the three space variable functions. The terms in square brackets refer to the physical and geometrical characteristics of the problem. K, G are the bulk and the shear moduli, respectively, of the elastic medium, whereas a, b are the dimensions of the rectangular region on which $P_{m,n}$ is applied. We must keep in mind that we deal with a saturated porous half-space, and the elastic coefficients have then to account for the compressibility of the porous phase, as described in the next section. However, according to the poroelastic model presented in Section 2.2, the loading surface affects the pore pressure through the undrained response of the porous medium and therefore we need to modify slightly Becker & Bevis (2004)'s approach. Moving from an elastic response to an undrained poroelastic response is done simply by replacing the elastic coefficients K, G in eq. (4) with their undrained equivalents K_u, G. The shear modulus G is considered as pore pressure-independent following Gassmann (1951) (see also the discussion by Berryman 2004). The total displacement field associated with the lake in undrained conditions is then obtained by summing the contribution of the whole set of rectangular regions used to discretize the surface of the lake (*a* and

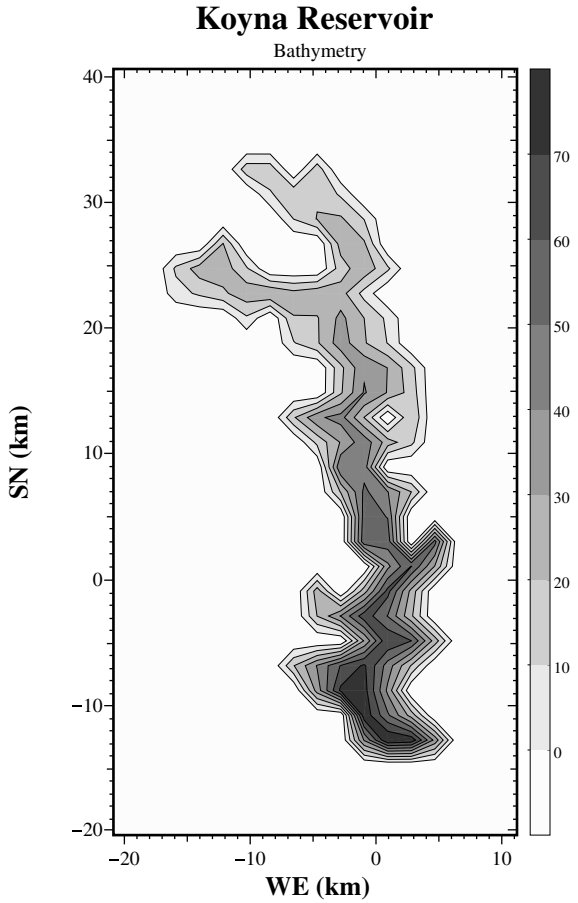

Figure 2. Bathymetry of the Koyna reservoir (in meters).

b are assumed to be constant throughout the lake discretization):

$$u_l^{tot}(x, y, z, t) = \Sigma_{m,n} P_{mn}(t) u^o_{l_{[K_u,G;a,b]}}(x - x_m, y - y_n, z), \tag{5}$$

for $1 \leq l \leq 3$.

The deformation and the stress fields are then derived from the usual expressions of elasticity. The stress field can be expressed as follows:

$$\sigma^r_{ij}(x, y, z, t) = \Sigma_{m,n} P_{mn}(t) \Psi_{ij_{[K_u,G;a,b]}}(x - x_m, y - y_n, z), \tag{6}$$

where Ψ_{ij} are functions of the partial derivatives of the displacement field. The superscript r is simply to remind us that these stresses are generated by the filling of the reservoir.

2.2 Poroelastic problem

To derive the appropriate equations of poroelasticity, we make use of the time derivative of the constitutive equation involving the mass of fluid, as established by Rice & Cleary (1976):

$$\frac{\partial m}{\partial t} = \frac{3\rho_f(\nu_u - \nu)}{2GB(1 + \nu)(1 + \nu_u)} \frac{\partial}{\partial t}\left(\sigma_{kk} + \frac{3P}{B}\right), \tag{7}$$

where m is the fluid mass content per unit volume of porous material, σ_{ij} the stress tensor and P is the pore pressure which can be broken down into the sum of a undrained term and a diffusive term, denoted here as P^d. Then, we express $\partial\sigma_{kk}/\partial t$ as the sum of two terms:

$$\frac{\partial \sigma_{kk}}{\partial t} = \frac{\partial \sigma^d_{kk}}{\partial t} + \frac{\partial \sigma^r_{kk}}{\partial t}. \tag{8}$$

The term σ^d_{kk} is the change in the confining pressure induced by fluid pressure. In the case of a uniform poroelastic medium of infinite extent, we can use the following formula (Pride *et al.* 2004) relating σ^d_{kk} to the diffusive contribution of fluid pressure change P^d:

$$\frac{\sigma^d_{kk}}{3} = -\frac{2}{B} \frac{\nu_u - \nu}{(1 + \nu_u)(1 - \nu)} P^d. \tag{9}$$

The term σ^r_{kk} refers to the stress induced by the reservoir loading as indicated in Section 2.1. To calculate its contribution in eq. (8), we consider the discrete time derivative $\frac{\Delta\sigma^r_{kk}}{\Delta t}$ resulting from the lake level change between t and $t + \Delta t$. Since we are dealing with a poroelastic medium, the above approach can be used only when the conditions for an undrained elastic behaviour are fulfilled. We derive $\frac{\Delta\sigma^r_{kk}}{\Delta t}$ from the expression of σ^r_{kk} in eq. (6):

$$\frac{\Delta \sigma^r_{kk}(x, y, z, t)}{\Delta t} = \Sigma_{m,n}\left[\frac{\Delta P_{m,n}(t)}{\Delta t}\right] \Psi_{kk_{[K_u,G;a,b]}}(x - x_m, y - y_n, z). \tag{10}$$

The conditions for undrained behaviour are satisfied for values of Δt such that the response is undrained throughout the crustal section. According to (2), $z_c \ll H$ implies $\Delta t \ll \frac{H^2}{4\pi c_p}$.

Let us now consider the conservation of fluid mass:

$$\frac{\partial q_i}{\partial x_i} + \frac{\partial m}{\partial t} = 0, \tag{11}$$

and the Darcy's law:

$$q_i = -\rho_f \frac{k}{\eta} \frac{\partial P}{\partial x_i}, \tag{12}$$

where q_i is the fluid mass flow rate, ρ_f the fluid density, k the permeability and η is the fluid viscosity.

After rearranging eqs (11) and (12) together with eqs (7), (8) and (9) and one gets:

$$\frac{\partial P}{\partial t} = \frac{2GB^2}{9} \frac{(1 + \nu_u)^2(1 - \nu)}{(1 - \nu_u)(\nu_u - \nu)} \frac{\partial}{\partial x_i}\left(\frac{k}{\eta} \frac{\partial P}{\partial x_i}\right) - \frac{B}{3}\left(\frac{\Delta\sigma^r_{kk}}{\Delta t}\right). \tag{13}$$

Assuming $k\eta^{-1}$ is constant, we obtain a diffusion equation with a hydraulic diffusivity:

$$c_p = \frac{2GB^2}{9} \frac{(1 + \nu_u)^2(1 - \nu)}{(1 - \nu_u)(\nu_u - \nu)} \frac{k}{\eta}. \tag{14}$$

However, the assumption of constant $k\eta^{-1}$ is invalid at the crustal scale, in particular because the porosity, and accordingly the permeability network as well, are reduced with increasing applied effective pressure $\sigma_e = -(\frac{\sigma_{kk}}{3} + P)$ (where again, $\sigma_{kk} = \sigma^r_{kk} + \sigma^d_{kk}$). For the sake of simplicity, we assume here a pressure dependence of porosity analogous to that suggested by Rice (1992):

$$\Phi = \Phi_o \exp\left(-\frac{\sigma_e}{K_p}\right), \tag{15}$$

where $K_p^{-1} = \Phi^{-1}(\frac{d\Phi}{d\sigma_e})$ is the compressiblity of the porous (fractured) medium. Note that K_p can be estimated from measurements in the laboratory, but is much more difficult to obtain at the field scale, so it is considered in the following as an unknown of the model. The porosity change under pressure also has direct consequences on the permeability. The main effect of effective pressure on fissures is to affect the fracture aperture w. According to Guéguen & Dienes (1989), we obtain $\Phi \propto w$ and $k \propto w^3$ in the case of fractured rocks, and hence, following (15), k varies with σ_e, so we can write:

$$k = k_o \exp\left(-\frac{3\sigma_e}{K_p}\right). \tag{16}$$

In eqs (15) and (16), Φ_o and k_o express the porosity and the permeability at zero effective pressure, respectively. These parameters are taken as constant throughout the crust. In the following, we also fix the viscosity at a typical value of mid-crustal conditions. However, we must bear in mind that the viscosity of water is mainly sensitive to temperature and decreases by one order of magnitude between the Earth's surface and a depth of 8 km. The decrease is abrupt in the first 5 km and much slower at greater depths. Finally, our approach amounts to considering that $k_o\eta^{-1}$ (i.e. the hydraulic conductivity at zero effective pressure) is constant throughout the crustal section. Although this is evidently an oversimplification, the effective pressure dependence given by eqs (15) and (16) indicates that the hydromechanical coupled processes are well accounted for and that the most appropriate poroelastic model is selected in compliance with these simplified assumptions. This is the same approximation as the one used by Rice (1992).

Walsh (1965) provides the following formula which relates the drained bulk modulus of the porous medium K to the bulk modulus of the solid phase K_s:

$$\frac{1}{K} = \frac{\Phi}{K_p} + \frac{1}{K_s}, \tag{17}$$

which allows us to calculate the value of the various hydromechanical parameters, using the classical expressions of elasticity and poroelasticity. Starting from the expressions given by Rice & Cleary (1976) for the poroelastic coefficients, we can rearrange the equations to obtain the expression of the Skempton coefficient:

$$B = \frac{K_p^{-1}}{K_p^{-1} + (K_f^{-1} - K_s^{-1})}, \tag{18}$$

Table 1. Table of the parameters used in numerical models.

Status	Model parameters	Numerical values
	Poroelastic/hydrodynamic parameters	
Fixed	G	1.5×10^{10} Pa
	K_s	4.54×10^{10} Pa
	K_f	3.33×10^{9} Pa
	Φ	0.01
	η	$2. \times 10^{-4}$ Pa s
Variable	K_p	$[7.9–1.5] \times 10^{9}$ Pa
	k_o	1.6×10^{-16} m^2
Calculated	B	[0.31–0.70]
	K	$[4.29–3.53] \times 10^{10}$ Pa
	K_u	$[4.37–4.17] \times 10^{10}$ Pa
	c_p	[0.20–0.09] m^2 s^{-1}
	Tectonic parameters	
Fixed	$\|\sigma_1 - \sigma_3\|$	60 MPa
	Friction coefficient	0.85

where K_f is the bulk modulus of the fluid. According to this equation, the Skempton coefficient is independent of the effective pressure σ_e. Other parameters which are used to calculate c_p vary as a function of porosity. Both the permeability and the specific storage of the medium are affected by the pressure dependence of the porosity. Table 1 reports the values of parameters used in the next sections. Elastic parameters (K_s, G) are those of Westerly Granite (see Rice & Cleary 1976) and the porosity has been fixed at a value $\Phi = 0.01$. Let us note that K_p is poorly constrained at the crustal scale. We consider here two values which lead, respectively, to two values of the Skempton coefficient, $B = 0.31$ and $B = 0.70$. Fig. 3 presents the relative variation of c_p, k and the specific storage S_s with depth ($\sim\sigma_e$) for the two values of K_p given in Table 1 (we assume here that the mean stress and the fluid pressure are lithostatic and hydrostatic, respectively). Not surprisingly, the pressure dependence of c_p is higher for large values of B, which coincide with an increased compressibility of the pores. Note that, for $B = 0.31$, the pressure dependence is very weak and is related to a highly incompressible porous phase.

2.3 Coulomb stress and failure criterion

The validity of a hydromechanical model depends on its ability to describe the spatial and temporal distributions of earthquakes during the observation period. Testing a model requires the definition of clear rules for accepting an event as 'positive' or as 'rejected', depending on the result of the test. Many authors have analysed the possible occurrence of seismic events by considering the evolution of the Coulomb Failure Function ΔCFF. We should point out that ΔCFF(t) is equivalent to CFF(t) − CFF(0). At $t = 0$, when the medium is still undisturbed by the stresses induced by the reservoir, CFF(0) results simply from the regional stress field. Thus, depending on the value of CFF(0), the initial system may be more or less close to rupture. ΔCFF is then indicative of how the disturbance (in this case, the reservoir filling) modifies the initial system. Depending on how this Coulomb stress evolves with time, the medium is either brought closer to failure (ΔCFF $>$ 0) or, on the contrary, becomes stabilized (ΔCFF $<$ 0). The Coulomb Failure Function is expressed as:

$$\mathrm{CFF} = \tau_{\vec{n},\vec{t}} + \mu(\sigma_{\vec{n}} + P), \tag{19}$$

where $\vec{n}$ and $\vec{t}$ represent the unit vector normal to the fault plane and the tangential unit vector in the slip direction, respectively, both oriented to yield the maximum CFF value. $\tau_{\vec{n},\vec{t}}$ and $\sigma_{\vec{n}}$ are the corresponding shear and normal stresses. Implicitly, the optimal Coulomb Failure Function criterion assumes that faults exist in all orientations in the medium. Of course, even though this may not be true, it is commonly assumed to make up for the lack of data. In the case of large events for which a focal mechanism is available, we can directly calculate the value of ΔCFF with the appropriate fault plane vectors and slip direction. In particular, this procedure was adopted for the M6.3 event of 1967 December 10.

Calculating the ΔCFF requires knowing the regional stress field, adding the contribution of the stress due to reservoir loading, and then calculating the resulting change in the Coulomb stress on the appropriate fault plane. The tectonic parameters used in the model are derived from the literature. The principal stresses $S1$ and $S3$ are considered as horizontal, whereas Gahalaut & Gahalaut (2008) propose an approximately N–S orientation of the main compressive stress. Moreover, according to Mandal *et al.* (2000) $|S_{Hmax} - S_{Hmin}| = 60$ MPa. The friction coefficient is set at $\mu = 0.85$ following Byerlee (1978). This latter parameter can evidently be highly variable in the crust. However, we have checked that taking other values does not significantly change the result. Moreover, this value is consistent with the orientation of the M6.3 fault which slipped in 1967 December 10 with respect to the tectonic stress field.

The rules for testing the validity of the model with respect to the seismological data are then as follow: let us consider a seismic

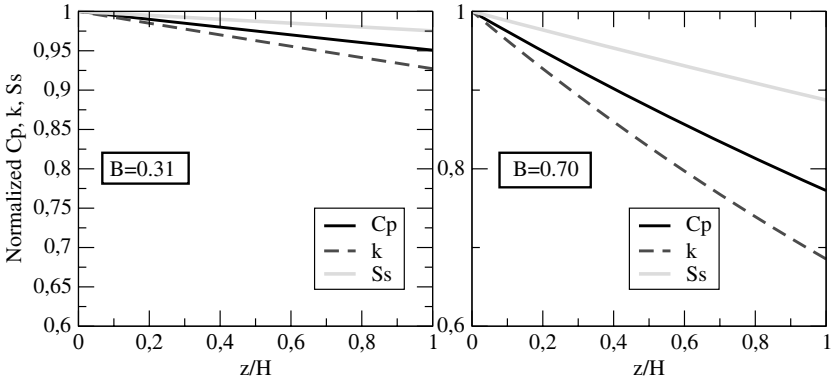

Figure 3. Variation of normalized value of c_p, k and S_s with normalized depth $\frac{z}{H}$ for the two values of K_p given in Table 1, corresponding to $B = 0.31$ and $B = 0.70$, respectively. For $\frac{z}{H} = 1$, the effective pressure is $\sigma_e \approx 200$ MPa.

event occurring at $t = t_n$, at the hypocentral location (x, y, z). This event can be accepted as 'positive', if and only if:

$$\Delta\mathrm{CFF}(x, y, z, t_n) > 0 \tag{20}$$

and

$$\Delta\mathrm{CFF}(x, y, z, t_n) > \Delta\mathrm{CFF}(x, y, z, t_m), \tag{21}$$

for whatever value of $t_m < t_n$. In other words, the event should be rejected if $\Delta\mathrm{CFF}(x, y, z, t_n)$ is negative or if a larger Coulomb Failure Function has been reached at this location at a previous time t_m. Indeed, in that case, the earthquake should rather trigger at t_m. This condition is fully consistent with the observations implying a Kaiser effect in the Koyna area as described in Section 1.1. However, a difficulty arises because the depth of each individual event is poorly constrained. Detailed analysis in the Koyna area indicates that most of the seismicity is located below a depth of 4 km (Talwani 1997a; Srinagesh & Rajagopala Sarma 2005). Accordingly, we adopt the following strategy: for each epicentral location (x, y) of events at time t, we examine $\Delta\mathrm{CFF}(x, y, z, t)$ for z ranging between 4 km and the bottom of the fluid-connected layer at H, investigating the depths at which the conditions defined in eq. (21) are satisfied at time t. Then, we select the value of z corresponding to a hypocentral depth yielding the maximum ΔCFF. Thus, if we fail to find a depth between 4 km and H satisfying the failure criterion, the event is given as 'rejected'.

2.4 Numerical procedure

The space is discretized with a 3-D rectangular grid, and we solve eq. (13) using the 3-D Alternating Direction Implicit method of Douglas & Rachford (1956), which is unconditionally stable. The condition $\Delta t \ll \frac{H^2}{4\pi c_p}$ defined in Section 2.2 is usually fulfilled for $\Delta t = 1$ day corresponding to the daily record of water-level variations of the lake, as long as $c_p < 10\,\mathrm{m^2\,s^{-1}}$. For higher values of c_p, we perform a linear interpolation of the daily sampling of the water-level record to fulfil the condition on Δt. We apply the finite difference scheme using the boundary and initial conditions defined later.

2.4.1 Boundary conditions

Impermeable conditions are applied at the base of the upper fluid-connected layer:

$$\partial P/\partial z = 0. \tag{22}$$

The vertical boundaries are sufficiently far not to be disturbed, so we impose:

$$\Delta P \approx 0. \tag{23}$$

At the surface, the free boundary conditions apply everywhere except below the reservoir. This can be written as

$$P(x_m, y_n, 0, t) = \rho_f g_o h_{m,n}(t), \tag{24}$$

where $h_{m,n}(t)$ is the column of water above the point (x_m, y_n) at time t, as defined in eqs (3).

2.4.2 Initial conditions

At $t = 0$ the reservoir is empty and we assume that the mean stress is lithostatic and the fluid pressure is hydrostatic. Therefore, $\sigma_e = (\rho - \rho_f)gz$ where ρ is the density of the crustal rocks. This allows us to calculate the various parameters as a function of the effective pressure (and accordingly to depth) as we do in Fig. 3.

2.5 Poroelastic response to water loading

Figs 4 and 5 show how the poroelastic response to water loading varies with space and time as a function of the diffusivity. We use the values of parameters given in Table 1. The fixed value of porosity $\Phi = 0.01$ can be considered as typical of crystalline rocks. In the simulations the Skempton coefficient is $B = 0.31$, $k_o = 1.6 \times 10^{-16}$ m^2 and the fluid viscosity has been fixed to a value $\eta = 2 \times 10^{-4}$ Pa s. This value is considered as typical of temperature $T = 150^\circ$, that is a depth of around 5 km. Since seismic events are mainly confined between 4 and 12 km, the fixed value for the viscosity is simply chosen to be representative of this range of depths. These values lead a value of diffusivity of $c_p = 0.2\,\mathrm{m^2\,s^{-1}}$. In the following, we present the results as a function of c_p. The reader should bear in mind that, when we speak about c_p, we refer to the values at zero effective pressure. Fig. 4 shows the normalized fluid pressure $P.P_o^{-1}$ on an E–W cross-section ($y = -10$ km in Fig. 2) at the peak of water level at $t = 817$ days (where $P_o = \rho_f gh(t = 817$ days) is the loading of the water column at the deepest point of the reservoir). The grey zones represent the pore pressure field in the undrained case, which is compared with the pore pressures associated with a diffusivity $c_p = 0.2\,\mathrm{m^2\,s^{-1}}$ whose isovalues are contoured by solid black lines. We observe that the isovalues for $c_p = 0.2\,\mathrm{m^2\,s^{-1}}$ spread deeper than for the undrained case down to mid-crustal depths. For distances such that $P = 0.01P_o$, the responses in the two cases are indistinguishable.

Fig. 5 shows the calculated results of fluid pressure and Coulomb stress change at the epicentral coordinate of the M6.3 event of 1967 December 10 at a depth of 5 km. The poroelastic parameters are those given in Table 1, and we consider five values of c_p in the range $0.01\,\mathrm{m^2\,s^{-1}}$ to $100\,\mathrm{m^2\,s^{-1}}$. We compare these curves with the water-level fluctuations and the undrained response. Finally, the porous medium can be regarded as a low-pass dephasing filter whose parameters are controlled by the poroelastic properties of the medium. These characteristics are well illustrated in Fig. 5. For

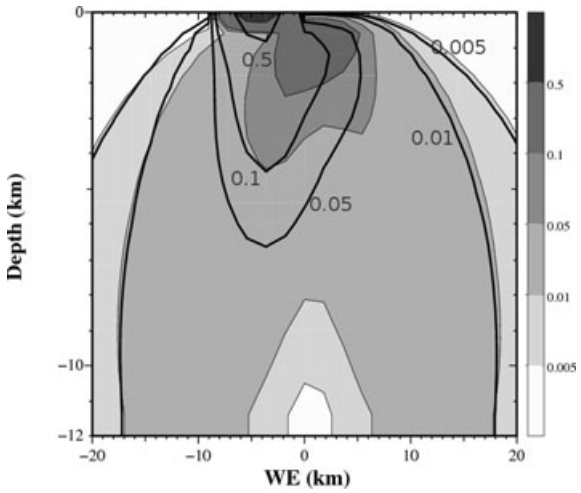

Figure 4. W–E (y = −10 km) cross-section (see Fig. 2) of normalized fluid pressure at time $t = 817$ days, for the undrained case (grey zones) and for $c_p = 0.2\,\mathrm{m^2\,s^{-1}}$ (black contours). Below the reservoir, the fluid pressure is higher at mid-crustal depth for $c_p = 0.2\,\mathrm{m^2\,s^{-1}}$. At distances such that the normalized pressure is lower than 0.01, the diffusive component is negligible and the response is dominated by the undrained contribution.

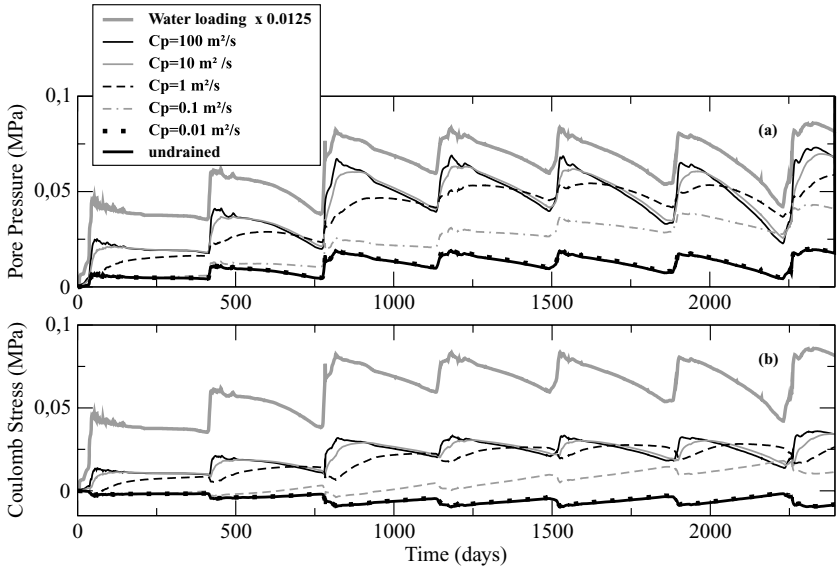

Figure 5. Time variation of pore pressure and Coulomb stress at the epicentral coordinate of the M6.3 event of 1967 December 10 at a depth of 5 km, for various values of c_p. This is compared with the water loading curve (solid grey line) and the undrained curve (solid black thick line).

$c_p = 100\,\mathrm{m^2\,s^{-1}}$, a comparison with the water loading curve shows that the phase lag is very short, since the fluid is allowed to diffuse rapidly into the porous medium. For $c_p = 1\,\mathrm{m^2\,s^{-1}}$, we observe that the annual fluctuations are strongly delayed, with a phase lag around 100–150 days at these depths. For $c_p = 0.1\,\mathrm{m^2\,s^{-1}}$, the water level fluctuations at an annual scale are strongly filtered. The pore pressure signal reflects mainly the low-frequency component, which increases as the reservoir fills up. The small fluctuations of pressure occurring in phase with the water-level signal are due to the elastic effect of water loading, which does not show any phase lag with respect to the water-level fluctuations. For $c_p = 0.01\,\mathrm{m^2\,s^{-1}}$, the pore pressure at 5 km depth is almost indistinguishable from the undrained response. This indicates that the critical depth z_c is shallower than 5 km.

As far as the Coulomb stress is concerned, the variations show similar effects as seen for the pore pressure. Since the Coulomb stress is very sensitive to the fluid pressure increase, we observe that higher Coulomb stress is obtained in high-permeability regimes. Around $c_p = 0.1\,\mathrm{m^2\,s^{-1}}$ the Coulomb stress increases as a result of reservoir filling. At lower c_p values, the Coulomb stress is negative, which precludes the possibility of seismic events being triggered at this location under this diffusion regime. Note that, here, we investigate the role of diffusivity by varying the permeability of the medium. However, K_p also has strong influence on the response of the medium, because it affects the poroelastic coefficients and particularly B. As mentioned earlier, by varying K_p and maintaining c_p constant (by changing the value of permeability), the $1\,D$ response in eq. (1) indicates that the pore pressure depends directly on the undrained term $b_1 = [B(1+\nu_u)][3(1-\nu_u)]^{-1}$. Thus, changing K_p may significantly affect the fluid pressure and hence the Coulomb stress, which depends on the effective pressure.

3 APPLICATION TO THE STUDY OF SEISMICITY IN KOYNA

3.1 Selection of the best hydromechanical model

The rules for defining a successful event are set out in Section 2.3. Following these rules, the best hydromechanical model will provide the highest rate of 'positive' events. In the previous section, we mainly emphasize the role of diffusivity on the response of the system, by varying the permeability. However, we indicate that modifications of K_p are also likely to cause drastic changes in the behaviour of the system. Even though changing K_p also affects the value of c_p, the major point is that the undrained contribution increases together with the Skempton coefficient, and this leads to a quite different response. These various dependence of the poroelastic response have led us to look for the best hydromechanical model by varying both K_p (or equivalently B) and c_p. Finally, when comparing two models yielding an equivalent success rate, we shall prefer the model which, on average, gives the highest values of ΔCFF for the whole set of events.

The best success rate is obtained for values of $c_p = 0.2\,\mathrm{m^2\,s^{-1}}$ ($k \approx 1.6 \times 10^{-16}\,\mathrm{m^2}$) and a bulk modulus of the porous phase $K_p = 7.9 \times 10^9$ Pa, leading to $B = 0.31$ (Figs 6a and b). Using these parameters, 51 out of 60 events (i.e. 85 per cent, after removal of events whose ERH error is too large, which is the case for 4 events out of 64) meet the defined selection criteria, which can be considered as a very successful result. However, we should note that the success rate is almost as good for $c_p = 0.15\,\mathrm{m^2\,s^{-1}}$ and $0.25\,\mathrm{m^2\,s^{-1}}$ (48/60 events, i.e. 80 per cent). For $c_p = 0.5\,\mathrm{m^2\,s^{-1}}$, the success rate is still $\approx$70 per cent but falls to $\approx$55 per cent for $c_p = 1\,\mathrm{m^2\,s^{-1}}$. We also observe a dramatic effect by changing K_p in the simulation to obtain $B = 0.7$, but keeping $c_p = 0.2\,\mathrm{m^2\,s^{-1}}$, with the success rate dropping to $\approx$15 per cent.

The error in determining the epicentral coordinates is likely to affect the results of the model. Even though these determination errors are not available for the studied period, a reasonable estimate, based on a later period, is $\pm$5 km. Using this estimate we are able to test our model by randomly distributing the epicentral coordinates within a 10 $\times$ 10 km square, which is centred on the determined epicentres. Ten random runs show that, using the above parameters, the model still produces an average success rate of $\approx$80 per cent which ensures the robustness of the determination of these parameters with regard to the seismological uncertainties.

Regarding the depth of events, they are continuously distributed between depths of 4 and 12 km with a predominance of events around depth of 4 km as shown in Fig. 6(b). However, we should

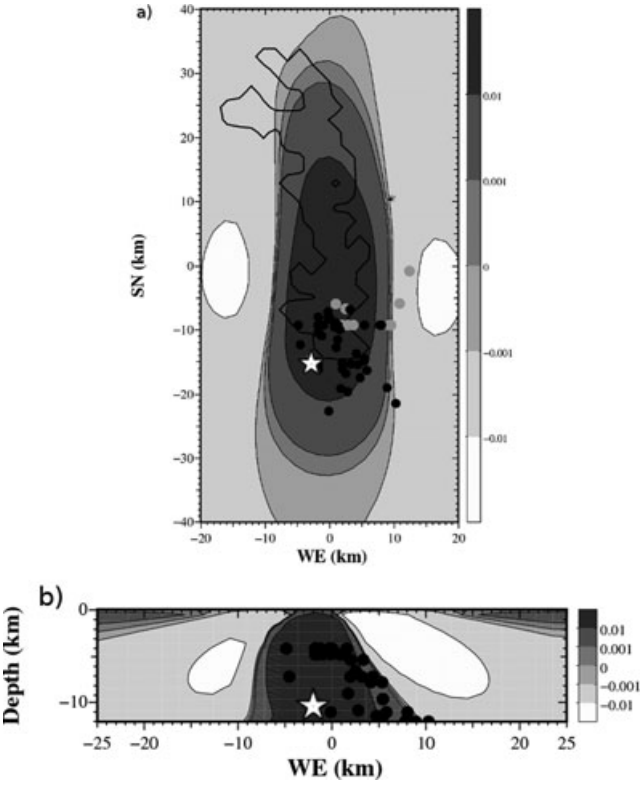

Figure 6. (a) Map of 'positive' (black circles) and 'rejected' (grey circles) events. The star indicates the epicentre of the major event of 1967 December 10. The locations of these events are compared with the Coulomb stress (in MPa) at the bottom of the poroelastic layer. The diffusivity c_p is set at $0.2\,\mathrm{m^2\,s^{-1}}$ and the B value at 0.31. 85 per cent of the seismic events are well accounted for by the model. (b) Depth distribution of 'positive' events (black circles). We assume that the events occur between −4 and −12 km, and the chosen depths are those which agree best with the rupture criterion.

remember that these depths correspond to those yielding the highest ΔCFF value. Even though it probably gives a somewhat biased picture of the real distribution of seismicity, the domain of depth variation is consistent with the seismological data. More reliable depth distribution data would mainly lead to slightly lower values of the average ΔCFF and the rate of successful events.

We do not apply the optimal Coulomb Failure Function criterion to the M6.3 major event, but rather make use of the ΔCFF in relation to the geometrical characteristics of the fault displacement, which in this case are known. By focusing on this particular event, we can corroborate the previous poroelastic model. The results are summarized on Fig. 7. First of all, it appears that there is a narrow range of c_p values from 0.15 to $0.25\,\mathrm{m^2\,s^{-1}}$ for which the Coulomb stress variation with time is consistent with the occurrence of a seismic event at a depth of 10 km at $t = t_E$. Fig. 7 reports the Coulomb stress change for $c_p = 0.2\,\mathrm{m^2\,s^{-1}}$ at a depth of 10 km, showing that the Coulomb stress is maximal at $t = t_E$. We compare the Coulomb stress variations at depths of 5 km and 10 km (the choice of a 5-km depth is arbitrary and is not intended to refer to any seismological data). We find the Coulomb stress is maximal at a depth of 10 km, whereas, at a depth of 5 km, it reaches a maximum 160 days before $t = t_E$. As a conclusion, the poroelastic model is fully consistent with the occurrence of the event at 10 km, and the model suggests that the event would trigger for ΔCFF ≈ 0.016 MPa.

The critical point here is the plausibility of the derived values for the hydromechanical and poroelastic parameters. As far as the poroelastic parameters are concerned, the bulk modulus of the porous phase leads to a Skempton coefficient $B = 0.31$. Is this value reasonable for crystalline rocks? Rice & Cleary (1976) indicate B values based on laboratory measurements ranging from 0.55 for Charcoal granite up to 0.85 for Westerly Granite. On the other hand, Talwani *et al.* (1999) have derived a Skempton coefficient of 0.66 from measurements in a well at Bad Creek Reservoir in South Carolina. In comparison with these values, $B = 0.31$ appears lower than expected. However, Roeloffs (1988) points out that poroelastic coefficients are strongly dependent on the confining pressure, and were measured at atmospheric pressure in the experiments of Rice & Cleary (1976). For Westerly granite, measurements of the bulk modulus give a Skempton coefficient of 0.55 at an effective pressure of 100 MPa and 0.23 at 200 MPa. Since seismicity around Koyna is located at depths below 4–5 km, the derived Skempton coefficient could be representative of conditions prevailing at these depths and is thus probably an entirely acceptable value for midcrustal pressure conditions.

The derived value of diffusivity c_p in the range 0.15 to $0.25\,\mathrm{m^2\,s^{-1}}$ should be compared with other values found in the Koyna area in particular and for RTS in general. As far as the Koyna area

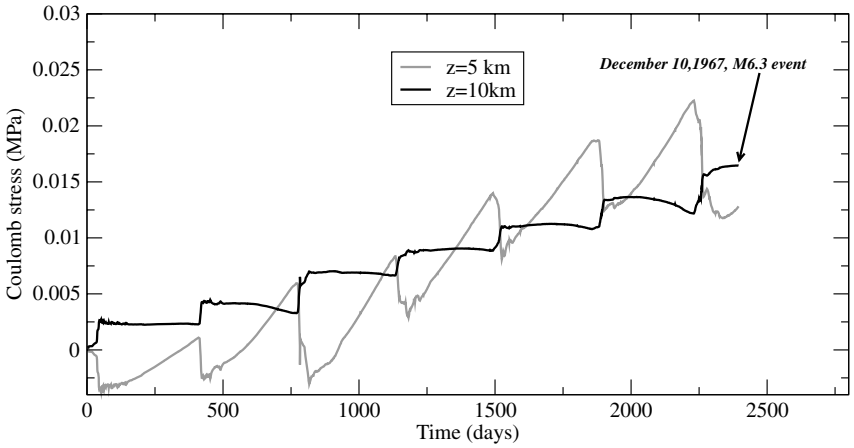

Figure 7. Time variation of Coulomb stress at location of the M6.3 event in 1967 December 10 ($t_E = 2395$ days after impoundment), at depth 10 km (black curve) for $c_p = 0.2\,\mathrm{m^2\,s^{-1}}$. This is compared with the response at 5 km depth (grey curve). At a depth of 5 km, the rupture criterion cannot be fulfilled at $t_E = 2395$ days, whereas the occurrence of a seismic event at t_E is consistent with a depth ≈10 km.

is concerned, Talwani (1981) derives a value of diffusivity $c_p = 0.13\,\mathrm{m^2\,s^{-1}}$ from an analysis of the epicentral area growth. Gupta & Rastogi (1976) provide values of $c_p = 0.58\,\mathrm{m^2\,s^{-1}}$ and $c_p = 1.72\,\mathrm{m^2\,s^{-1}}$ by analysing the time lag of seismicity with respect to the increase of water level. These methods evidently only crudely take account of the physics of the processes involved and thus they yield somewhat biased values. However, Talwani (1981) indicates that, whereas permeability in the crust covers many orders of magnitudes, the range of diffusivity values is very narrow when fluids are involved in seismogenic processes. Usually, the diffusivity ranges from 0.1 to $10\,\mathrm{m^2\,s^{-1}}$. In reservoirs, the diffusivity is found to vary from 0.02 to $12.5\,\mathrm{m^2\,s^{-1}}$, so our results lie in the lower range of observed values for RTS and are very consistent with the values given by Talwani (1981).

Another point of interest in our study is the distribution of ΔCFF predicted by the model. The value of ΔCFF responsible for triggering an earthquake is still a matter of debate. The correlation between the change of stress and the rate of seismicity is maintained for values as low as 1×10^{-2} MPa (Reasenberg & Simpson 1992; Stein *et al.* 1992; Harris *et al.* 1995; Hardebeck *et al.* 1998) but, according to the careful study of Ziv & Rubin (2000), a lower threshold for the triggering of an earthquake has not yet been demonstrated. As a consequence, we do not impose any lower threshold in our simulations. Fig. 8 reports ΔCFF as a function of time, showing 40 events (79 per cent) having values higher than 0.01 MPa. The Coulomb stresses lower than 0.01 MPa correspond to events that are the most distant from the lake. In our modelling, due to the Coulomb stress pattern, these events correspond to the deepest data points in Fig. 6. The average value of ΔCFF is around 0.04 MPa. Even though this value is small, it can still be considered as reasonable according to the references quoted earlier. Underestimating the depths of the events evidently has an influence on the value of the Coulomb stress at which events are triggered. In the absence of reliable hypocentral depths, we restrict our study to a homogeneous approach. The good success rate obtained should not mask the possible existence of a more complex hydraulic pattern. At least, the homogeneous approach seems to provide a good first-order hydraulic model.

3.2 Modelling the behaviour of the system following the M6.3 event of 1967 December 10

In this section, we aim to obtain a better understanding of the hydromechanical coupling in the Koyna area from an analysis of the mechanical effects following the major seismic event of magnitude 6.3 occurring in 1967 December 10. Until now, we have not considered the stress field changes possibly accompanying the occurrence of seismic events. Neglecting these stress perturbations is a reasonable assumption, since the dimension of the faults for events of magnitude ≤ 4 is less than or equal to the grid spacing. Moreover we do not have any information on their faults characteristics and focal mechanisms. On the contrary, the M6.3 event is likely to have strongly modified the stress field and, as a consequence, will affect the spatial and temporal distributions of the regional seismicity.

Considering the relocated events shown in Fig. 1(b), we observe that the M6.3 event is followed by a sequence of aftershocks. These relocated events provide an incomplete and possibly misleading view of the seismicity since the whole sequence of events is not considered. The temporal distribution of all the recorded events is reported in Fig. 9, together with the distribution of relocated events and the water-level variations. The reference time along the x axis corresponds to $t - t_E$. The aftershock sequences are usually fitted using an Omori law:

$$n(t - t_E) = K_o/(a + (t - t_E))^p, \tag{25}$$

where $n(t - t_E)$ is the number of aftershocks per unit time interval at time $t - t_E$ after the main event, p is the Omori exponent and the a value controls the shape of the decay law close to the onset time of the event. For the recorded data, we obtain: $a = 1.3$ days and a rather low $p = 0.88$, which leads to a relatively long duration of the earthquake sequence. We also note that there are no relocated events between $t - t_E = 85$ days and $t - t_E = 264$ days, and seven relocated events occurring after $t - t_E = 264$ days have a potential link with the peak of water level culminating at $t - t_E = 264$ days.

We examine here the possibility that the aftershocks result from fluid weakening processes due to the conjugated effects of the

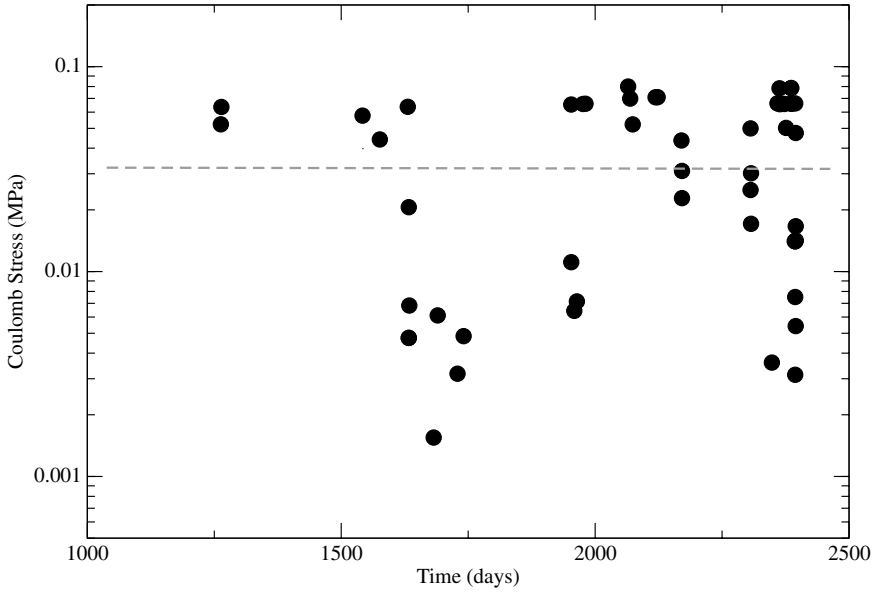

Figure 8. Distribution of the Coulomb stress for the various events versus time. The average value is ≈0.04 MPa and the Coulomb stress at failure is higher than 0.01 MPa for 79 per cent of events.

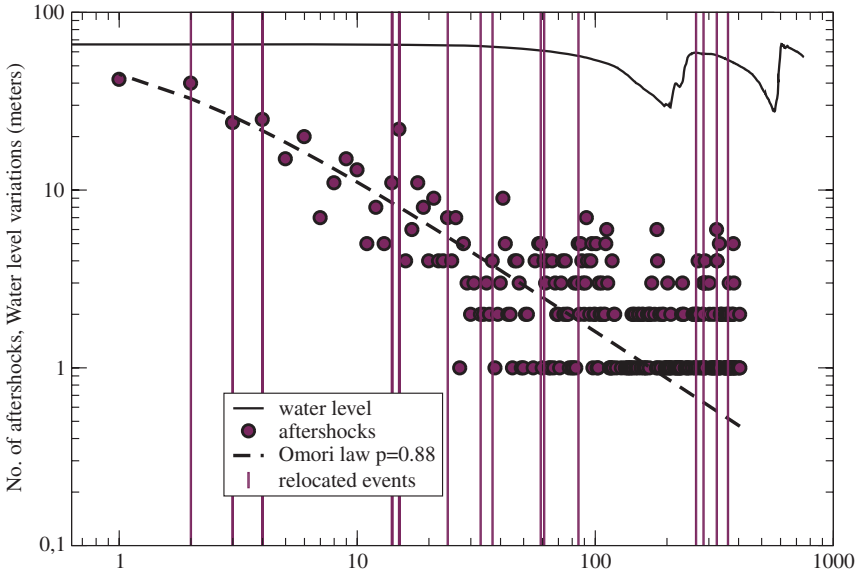

Figure 9. Number of aftershocks versus time fitted with an Omori law with $p = 0.88$ on a log–log plot. The figure also displays the position in time of the relocated events and the variation of level of the lake.

poroelastic post-seismic relaxation and water-level fluctuations of the lake. The hydrodynamic and the poroelastic parameters derived in Section 3.1 are then used to model the post-seismic evolution. The model needs to be consistent with the characteristics in space and time of the relocated events as well as the time dependence of the aftershocks. As far as the relocated events are concerned, the approach is similar to that described in the previous section, but we also need to consider the strain field associated with the fault motion of the M6.3 event.

Another approach is required to account for the time dependence of the whole sequence of aftershocks. Since we lack accurate information on the location of most of the events, we introduce some statistical elements into the mechanical model, as Gavrilenko (2005) which considers the poroelastic response to a fault slip. The time dependence of the Coulomb stress is controlled by the pressure gradient between the compressed and the dilated areas. Usually, we observe a relaxation of the number of aftershocks with time that can be analysed in terms of the Omori Law and compared with the observed sequences. Gavrilenko (2005) found that the decay law depends on the hydrodynamic properties of the medium. Let us note that, for simplicity, the stress field due to the aftershocks was not taken in account. Although this is likely to modify slightly the decay law, we have checked that this effect is very weak.

Both of these analyses require reliable fault slip models of the M6.3 event. Talwani (1997a) has compiled various inversions of the focal mechanism given by several seismologists. Except for Langston (1976), most authors agree on a left-lateral and westerly dipping strike-slip fault. Talwani (1997a) indicates that the strike of the fault plane is $\pm 10^\circ$ of N20° and that the fault dips to the north–west with an angle of between 66° and 80°. Moreover, Gupta *et al.* (1999) report a dip angle of 60° from the analysis of a drillhole in the fault segment. Accordingly, we assume a left-lateral strike-slip fault oriented N16° and dipping 60° to the W–NW. We adopt a fault length of $L = 15$ km consistent with the dimension of the North Escarpment Zone, which is one of the 3 clusters of events relocated by Srinagesh & Rajagopala Sarma (2005). We also assume a square geometry for the fault, providing us with a ratio $vL^{-1} = 6.6 \times 10^{-5}$ (where v is the average displacement along the fault), which lies in the range of values classically reported for active faults (Scholz 2002, e.g.). In addition, we consider an elliptic slip distribution along the fault plane, whose surface-area has been divided into 7×7 patches. Moreover, the fault position is chosen in such a way that the epicentre of the major event is positioned on the fault. Small variations of any one of the parameters may affect the success rate of the model, because there are very sharp changes in the strain field resulting from slip displacement of the fault. Let us note that events located very close to the fault are, in particular, strongly affected by the choice of the slip pattern and that for these events the dislocation models are hardly acceptable.

3.2.1 Results using the parameters determined in Section 3.1

According to our modelling, 65 per cent (i.e. 17/26) of relocated post-seismic events are compatible with the model as shown in Fig. 10. To identify possible trends in the behaviour of the system, Fig. 11 shows the instantaneous success rate $IR(t - t_E)$ (i.e. the number of 'positive' events/ the number of relocated events that have already occurred between t_E and $t - t_E$). The dashed line (corresponding to $c_p = 0.2\,\mathrm{m^2\,s^{-1}}$) shows that, for the first 100 days after the major earthquake, 72 per cent of relocated events are well-described by this fault model. After $t - t_E \approx 100$ days, the success rate decreases slightly and only 3/7 events are positive. Seven events are clearly not sufficient to draw conclusions on a statistical basis. Nevertheless, it appears that the occurrence of positive events after $t - t_E = 264$ days is directly related to the slow pore pressure relaxation resulting from $c_p = 0.2\,\mathrm{m^2\,s^{-1}}$. Full poroelastic relaxation is not reached after one and a half years. This represents a possible mechanism for triggering late events.

In a second test for validating the model, we compare the decay of the whole sequence of aftershocks with synthetic sequences generated by modelling using the same approach as Gavrilenko (2005). With $a = 2.5$ days and $p = 0.67$ (Fig. 12, square symbols), it appears that the population of aftershocks in the synthetic sequence decreases too slowly compared to the observed records. As a consequence, we can reject this model, which is inappropriate to describe all the characteristics of the post-seismic response.

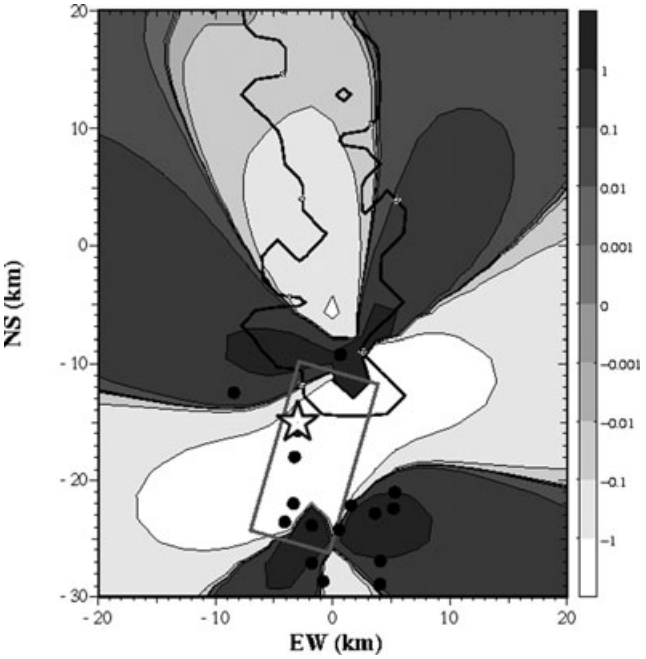

Figure 10. Map of 'positive' seismic events (black circles) and Coulomb stress (in MPa) at depth 5 km. The projection of the fault to the surface is represented by a grey rectangle and the position of the main shock with a star symbol.

3.2.2 Model considering a jump in permeability

The main shock disturbs the neighbourhood of the slipping fault and may induce some modifications of the hydromechanical properties. Permeability changes have been reported by various authors as resulting from the shaking of aquifers by earthquakes (Rojstaczer *et al.* 1995; Tokunaga 1999; Roeloffs 1998; Gavrilenko *et al.* 2000; Charmoille *et al.* 2005). Moreover, Talwani (2000) suggests that the lack of shallow seismicity observed for $M > 3$ events could be associated with a permeability enhancement caused by the M6.3 event. Here, we assume here that there is a sharp change in permeability resulting from the inelastic deformation of the medium. Thus, the diffusivity is constant and equal to $0.2\,\mathrm{m^2\,s^{-1}}$ before the M6.3 event, and then jumps to a new value, which is yet to be determined, just after the event. In Fig. 9, we report the decay law corresponding to $c_p = 2.5\,\mathrm{m^2\,s^{-1}}$($k_o = 2.0 \times 10^{-15}\,\mathrm{m^2}$, i.e. an increase of k by a factor of 12.5), showing that the aftershock decay is similar to the observations, with $a = 2.1$ days and $p = 0.87$. On the other hand, this new model must be confronted with the spatio-temporal distribution of the relocated events (Fig. 11). For $t - t_E < 100$ days, the success rate is $IR(t - t_E) = 79$ per cent (black curve), that is better than for $c_p = 0.2\,\mathrm{m^2\,s^{-1}}$ (dashed curve). However, the model does not allow us to predict the late events ($t - t_E \geq 264$ days). The explanation is that the poroelastic relaxation is fully achieved at this time, so the driving force for triggering an event is no longer active. The water-level fluctuations for this period do not seem to be sufficient to trigger seismic events. Nevertheless, it is interesting to compare the value $c_p = 2.5\,\mathrm{m^2\,s^{-1}}$ with the value found by Talwani (1981) for the period October 1967–April 1968. Using the same approach as for the value quoted in Section 3.1, Talwani (1981) derives a value of diffusivity $c_p = 12.48\,\mathrm{m^2\,s^{-1}}$, that is 5 times higher than our result. In spite of this difference, both approaches suggest an increase of diffusivity associated with the occurrence of the major shock.

4 DISCUSSION

In this study, we demonstrate that a c_p value of $0.2\,\mathrm{m^2\,s^{-1}}$ is appropriate to describe the seismicity for $t < t_E$ in relation with the lake-level fluctuations. Fig. 1(a) shows that the seismic activity migrates toward the south after t_E, whereas Fig. 10 indicates that the M6.3 earthquake has a strong affect on the pattern of post-seismic activity. This observation has also been pointed out by Gahalaut *et al.* (2004). However, even if the post-seismic events fall within the positive Coulomb lobes, since these events are delayed, they require a time-dependent process to be triggered. Such a process is provided here by the re-equilibration of fluids from the compressed to the dilated area, as suggested by Nur & Booker (1972) and more recently by Bosl & Nur (2002) and Gavrilenko (2005). In

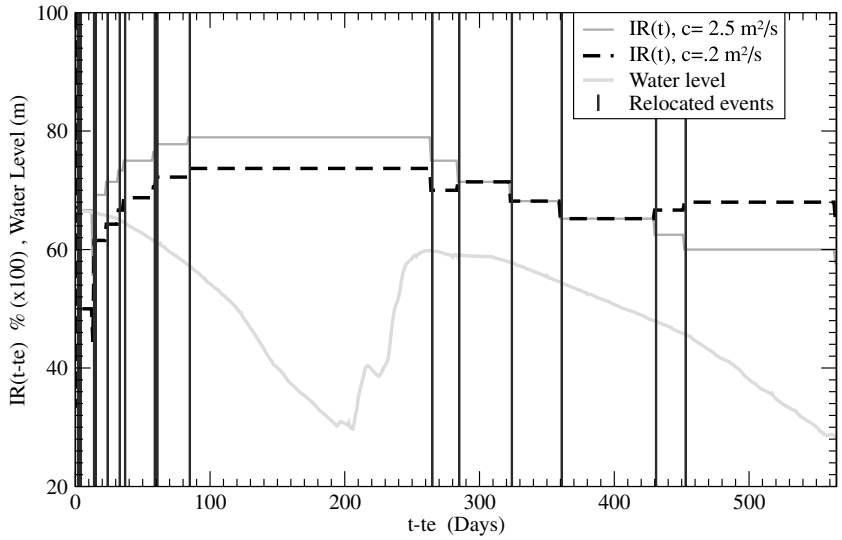

Figure 11. Instantaneous success rate obtained with two models, with $c_p = 0.2\,\mathrm{m^2\,s^{-1}}$ and $c_p = 2.5\,\mathrm{m^2\,s^{-1}}$. With $c_p = 0.2\,\mathrm{m^2\,s^{-1}}$, the model gives a success rate of 65 per cent. For $t - t_E > 264$ days, the poroelastic relaxation is not complete and the model agrees with 3 out of 7 events. With $c_p = 2.5\,\mathrm{m^2\,s^{-1}}$, the model predicts 79 per cent of events for $t - t_E < 100$ days but cannot predict the late events when $t - t_E > 264$ days.

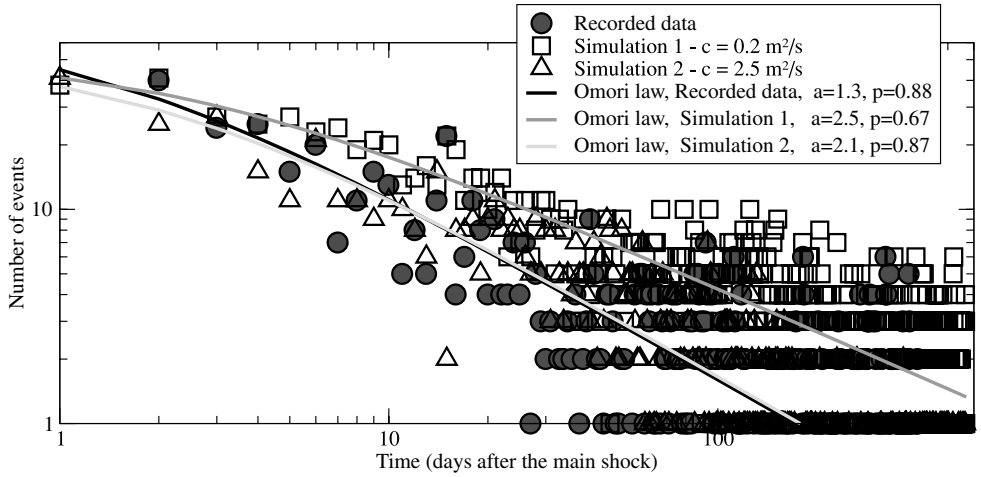

Figure 12. Comparison between the decay of recorded sequences of aftershocks (grey circles) and synthetic models (squares and triangles up). We note that the model with $c_p = 0.2\,\mathrm{m^2\,s^{-1}}$ displays a excessive slow decrease ($p = 0.67$) whereas the model with $c_p = 2.5\,\mathrm{m^2\,s^{-1}}$ is in a good agreement ($p = 0.87$) with the observations.

our modelling, there is an apparent discrepancy between the diffusivity values derived before and after t_E. A c_p value of $2.5\,\mathrm{m^2\,s^{-1}}$ agrees relatively well with the aftershock sequences, suggesting a jump in permeability associated with the M6.3 event. However, this diffusivity value still poorly matches the data for $t - t_E \geq 264$ days.

Even though various post-seismic processes may occur, we restrict ourselves to considering the mechanical effect of lake fluctuations and poroelastic relaxation. To understand the spatio-temporal distribution for $t - t_E \geq 264$ days, we may need to relax the assumption of homogeneous permeability in view of seismological arguments and field observations. From a seismological point of view, the observations show a contrast in spatial and temporal distribution. Just after t_E, the aftershocks are located mainly in the southern positive lobe of the Coulomb stress field. On the contrary, for $t - t_E > 264$ days, 5 out of 7 relocated events are situated in the neighbourhood of the northern positive lobe. As far as the field observations are concerned, the southern lobe corresponds to the intersection between NE–SW and NW–SE trending fault systems as shown in Fig. 1(a). Talwani (1997a) reports various observations from a GSI Report[1] and Sathe *et al.* (1968), which were carried out following the main shock. In particular, a spatially continuous zone of fissures associated with the M6.3 earthquake, and extending over an area of several km, has been identified east of the KRFZ zone (see Fig. 1a). Thus, we have good grounds for assuming that fluid flow is enhanced in this area and that this influences the spatio-temporal distribution of aftershocks. We propose here that the medium is composed of two compartments with different hydrodynamic properties as shown in Fig. 13. The diffusivity in the white northern zone is not modified by the M6.3 event, with c_p set at $0.2\,\mathrm{m^2\,s^{-1}}$, whereas the grey southern zone exhibits a jump of diffusivity and accordingly, c_p is set at $3.5\,\mathrm{m^2\,s^{-1}}$. The higher diffusivity in the grey area leads to processes with short time constants, which control the decay of aftershocks, whereas the lower diffusivity in the white zone affects the late-stage behaviour of the system and favours the occurrence of seismic events at $t \geq 264$ days. Fig. 14 summarizes the results of this hydromechanical model. We obtain a decay law

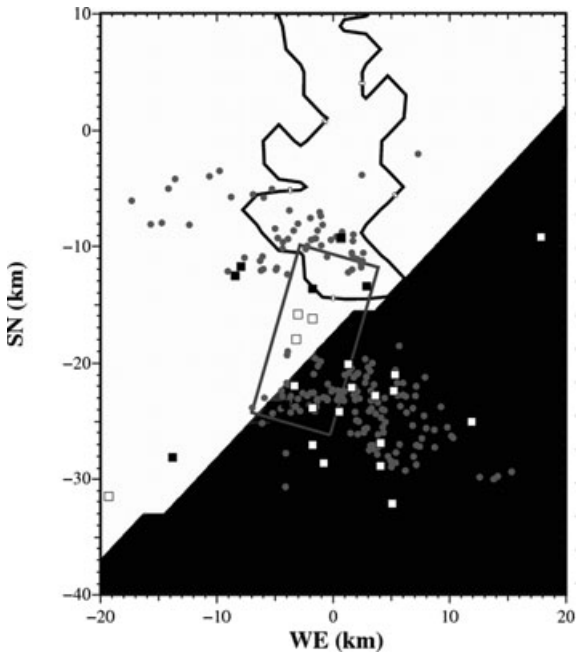

Figure 13. Synthesis of the results for the model with two hydrological compartments. The white and the black zones correspond to $c_p = 0.2\,\mathrm{m^2\,s^{-1}}$ and $c_p = 3.5\,\mathrm{m^2\,s^{-1}}$ respectively. The relocated events are plotted as white squares for $t - t_E < 100$ days and as black squares for $t - t_E > 264$ days. The grey dots correspond to a synthetic sequence of aftershocks generated by poroelastic modelling. This simulation shows that aftershocks are more numerous in the grey zones. This effect is even amplified when looking at seismicity for $t - t_E < 100$ days. Moreover the spatial distribution of synthetic aftershocks agrees rather well with the position of the relocated events.

which matches the observations relatively well, and a success rate of 69 per cent (i.e. 18/26 events), which is better than the two earlier homogeneous models. Moreover, in view of the statistical distribution of aftershocks generated with our poroelastic model (grey dots on Fig. 13), we observe that the synthetic sequence exhibits a contrast from north to south, which is qualitatively similar to the observations.

[1]A Geological Report on the Koyna Earthquake of 11th December 1967, Satara District, Maharashtra State. Geological Survey of India, unpublished.

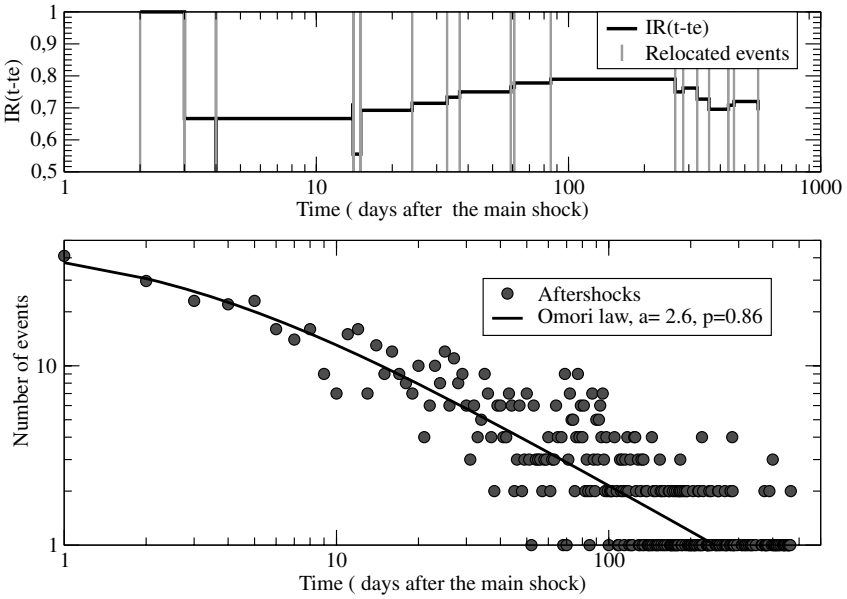

Figure 14. Instantaneous success rate $IR(t - t_E)$ and decay of the number of aftershocks with time, for the two compartments model shown in Fig. 13. The final success rate in predicting events following the main shock is ≈69 per cent and we can see that the late-stage events can be accounted for with this model (with a mitigated success as observed with for the homogeneous model when using $c_p = 0.2\,\mathrm{m^2\,s^{-1}}$), whereas the Omori exponent agrees with the observations, with $p = 0.86$.

Nevertheless, different hydrological models could give equivalent results provided they display contrasting behaviours from north to south across the area. In our model, fluids flow through a southern fracture zone, which is more permeable than the northern zone, and the diffusivity derived from the aftershock sequence is mainly representative of this fracture zone. The dynamics of the system for the period after the main shock is controlled by a diffusion coefficient $c_p = 0.2\,\mathrm{m^2\,s^{-1}}$. This value of c_p implies that the time constant of poroelastic relaxation is much higher than the annual period of lake-level fluctuation. Using a cross-correlation analysis Pandey & Chadha (2003) obtained a good correlation between the seismicity and the water-level fluctuations, except in the time window from 1968 to 1973, which was strongly disturbed by the occurrence of the major shock. This provides an indication for the time constant of the relaxation process which is consistent with $c_p = 0.2\,\mathrm{m^2\,s^{-1}}$.

Owing to fracturing processes and subsequent fracture healing and sealing, permeability is likely to change in space as a function of the heterogeneities and time. Our study emphasizes the contrast between the values of the diffusion coefficient before and after the major event, as already demonstrated by Talwani (1981). However, many time-dependent processes (afterslip, viscoelastic, coupling, etc.) quoted in the literature predict aftershock sequences with the appropriate Omori parameters. It is still possible that the decay of aftershocks is mainly controlled by such processes, thus overcoming the poroelastic relaxation, up to a given time $t - t_E$ beyond which fluid circulation is again effective. However, such processes still need to explain the contrast between the northern and the southern zones. Our model is likely to be validated or rejected by modelling the evolution of the system after our period of investigation. Among many other points, the persistence of the system and the evolution of seismicity are crucial factors. As discussed earlier, the major seismic event has a strong effect on the pattern of seismicity following the main shock, and the Coulomb stress associated with this event dominates the Coulomb stress due to lake-level fluctuations. To check that fluctuations of lake level could again play an active mechanical role, we need to envisage healing processes and a relaxation of Coulomb stress with time constants that are consistent with the seismicity pattern.

5 CONCLUSION

In this study, we develop various poroelastic models to describe the occurrence of RTS in the Koyna Area over the first eight years of seismic activity. We are mainly concerned with the following two periods.

(1) For the period before the M6.3 earthquake of 1967 December 10, we derive a homogeneous poroelastic model that explains more than 80 per cent of the relocated events. The model that best fits the data assumes a diffusivity, c_p, of $0.2\,\mathrm{m^2\,s^{-1}}$ and a Skempton coefficient, B, of 0.31. The average Coulomb stress threshold for earthquake triggering is around 0.04 MPa.

(2) Following the M6.3 event, we observe a southward migration of seismic events. To match the aftershock decay rate, we consider a diffusivity of around $2.5\,\mathrm{m^2\,s^{-1}}$ after the M6.3 event. This implies that permeability consecutive to the major event increases by a factor of 12.5. This model gives relatively good results for the first few months following the main earthquake, but appears inadequate to describe the late-stage relocated events that appear around 9 months after the main shock. Because of this, we recognize that the homogeneous hydrological model is too simplified to account for the complexity of the fluid-assisted processes after the major earthquake. Accordingly, we propose a model with two compartments having contrasting diffusivities, with fluid flow in the southern zone being enhanced as a result of damage after the main shock. This model provides a reasonably good simulation of the hydromechanical processes for one and a half years after the major event.

ACKNOWLEDGMENTS

The authors thank the Director of the National Geophysical Research Institute, CSIR, for his kind permission to publish this work. CS acknowledges the financial support provided by CSIR. Dr P.K. Naik kindly answered our questions on the geometry of the Koyna reservoir. We are also grateful to two anonymous reviewer, and Professor H.J. Kümpel, for their thorough and constructive reviews. Dr M.S.N. Carpenter post-edited the English style.

REFERENCES

Becker, J.M. & Bevis, M., 2004. Love's problem, *Geophys. J. Int.,* **156,** 171–178.

Berryman, J.G., 2004. Poroelastic shear modulus dependence on pore-fluid properties arising in a model of thin isotropic layers, *Geophys. J. Int.,* **157,** 415–425.

Bosl, W.J. & Nur, A., 2002. Aftershocks and pore fluid diffusion following the 1992 Landers earthquake, *J. geophys. Res.,* **107,** 2366–2368.

Byerlee, J., 1978. Friction of rocks, *Pure appl. Geophys.,* **116,** 615–626.

Charmoille, A., Fabbri, O., Mudry, J., Guglielmi, Y. & Bertrand, C., 2005. Post-seismic permeability change in a shallow fractured aquifer following a M_L 5.1 earthquake (Fourbanne karst aquifer, Jura outermost thrust unit, eastern France), *Geophys. Res. Lett.,* **32,** L18406, 18406–18411, doi:10.1029/2005GL023859.

do Nascimento, A.F., Lunn, R.J. & Cowie, P.A., 2005a. Numerical modelling of pore-pressure diffusion in a reservoir-induced seismicity site in northeast Brazil, *Geophys. J. Int.,* **160,** 249–262.

do Nascimento, A.F., Lunn, R.J. & Cowie, P.A., 2005b. Modeling the heterogeneous hydraulic properties of faults using constraints from reservoir-induced seismicity, *J. geophys. Res.,* **110,** B09201, doi:10.1029/2004JB003398.

Douglas, J. & Rachford, H., 1956. On the numerical solution of the heat conduction problem in 2 and 3 space variables, *Trans. Am. Math. Soc.,* **82,** 421–439.

Duncan, R.A. & Pyle, D.G., 1988. Rapid eruption of the Deccan flood basalts at the Cretaceous/Tertiary boundary, *Nature,* **333,** 841–843.

Gahalaut, K. & Gahalaut, V.K., 2008. Stress triggering of normal aftershocks due to strike slip earthquakes in compressive regime, *J. Asian Earth Sci.,* **33,** 379–382.

Gahalaut, V.K., Kalpana, & Singh, S.K., 2004. Fault interaction and earthquake triggering in the Koyna-Warna region, India, *Geophys. Res. Lett.,* **31,** L11614, 11614–11618, doi:10.1029/2004GL019818.

Gassmann, F., 1951. ber die Elastizit poroser Medien, *Veirteljahrsschrift der Naturforschenden Gesellschaft in Zurich,* **96,** 1–23.

Gavrilenko, P., 2005. Hydromechanical coupling in response to earthquakes: on the possible consequences for aftershocks, *Geophys. J. Int.,* **161,** 113–129.

Gavrilenko, P., Melikadzé, G., Chélidzé, T., Gibert, D. & Kumsiashvili, G., 2000. Permanent water level drop associated with the Spitak Earthquake: observations at Lisi Borehole (Republic of Georgia) and modelling, *Geophys. J. Int.,* **143,** 83–98.

Guéguen, Y. & Dienes, J., 1989. Transport properties of rocks from statistics and percolation, *Math. Geol.,* **21,** 1–13.

Gupta, H. & Rastogi, B., 1976. *Dams and Earthquakes,* Elsevier, New-York.

Gupta, H.K. & Rastogi, B.K., 1974. Will another damaging earthquake occur in Koyna? *Nature,* **248,** 215–216.

Gupta, H.K. *et al.*, 1999. Anatomy of surface rupture zones of two stable continental region earthquakes, 1967 Koyna and 1993 Latur, India, *Geophys. Res. Lett.,* **26,** 1985–1988.

Gupta, H.K., Mandal, P. & Rastogi, B.K., 2002. How long will triggered earthquakes at Koyna, India continue, *Curr. Sci.,* **82,** 202–210.

Hardebeck, J.L., Nazareth, J.J. & Hauksson, E., 1998. The static stress change triggering model: Constraints from two southern California aftershock sequences, *J. geophys. Res.,* **103,** 24 427–24 438.

Harris, R.A., Simpson, R.W. & Reasenberg, P.A., 1995. Influence of static stress changes on earthquake locations in southern California, *Science,* **375,** 221–224.

Kalpna & Chander, R., 2000. Green's function based stress diffusion solutions in the porous elastic half space for time varying finite reservoir loads, *Phys. Earth planet. Inter.,* **120,** 93–101.

Langston, C.A., 1976. A body wave inversion of the Koyna, India, earthquake of December 10, 1967, and some implications for body wave focal mechanisms, *J. geophys. Res.,* **81,** 2517–2530.

Lee, W.H.K. & Raleigh, C.B., 1969. Fault-plane Solution of the Koyna (India) Earthquake, *Nature,* **223,** 172–173.

Mandal, P., Rastogi, B.K. & Gupta, H.K., 2000. Recent Indian earthquakes, *Curr. Sci.,* **79,** 1334–1346.

Naik, P., Awasthi, A., Anand, A.V.S.S. & Mohan, P., 2001. Hydrogeologic framework of the Deccan terrain of the Koyna River basin, India, *Hydrogeology J.,* **9,** 243–264.

Neuman, S.P., 1990. Universal Scaling of Hydraulic Conductivities and Dispersivities in Geologic Media, *Water Resour. Res.,* **26,** 1749–1758.

Nur, A. & Booker, J.R., 1972. Aftershocks Caused by Pore Fluid Flow? *Science,* **175**(4024), 885–887.

Pandey, A.P. & Chadha, R.K., 2003. Surface loading and triggered earthquakes in the Koyna-Warna region, western India, *Phys. Earth planet. Inter.,* **139,** 207–223.

Pride, S.R., Moreau, F. & Gavrilenko, P., 2004. Mechanical and electrical response due to fluid-pressure equilibration following an earthquake, *J. geophys. Res.,* **109,** B03302, doi:10.1029/2003JB002690.

Rajendran, K. & Harish, C.M., 2000. Mechanism of triggered seismicity at Koyna: an assessment based on relocated earthquake during 1983-1993, *Curr. Sci.,* **79,** 358–363.

Reasenberg, P.A. & Simpson, R.W., 1992. Response of regional seismicity to the static stress change produced by the Loma Prieta earthquake, *Science,* **255,** 1687–1690.

Rice, J.R., 1992. Fault Stress States, Pore Pressure Distributions, and the Weakness of the San Andreas Fault, in *Fault Mechanics and Transport Properties in Rocks,* pp. 475–503, eds Evans, B. & Wong, T.-F., Academic Press, San Francisco.

Rice, J.R. & Cleary, M.P., 1976. Some Basic Stress Diffusion Solutions for Fluid-Saturated Elastic Porous Media With Compressible Constituents, *Rev. Geophy. Space Phys.,* **14,** 227–241.

Roeloffs, E.A., 1988. Fault stability changes induced beneath a reservoir with cyclic variations in water level, *J. geophys. Res.,* **93,** 2107–2124.

Roeloffs, E.A., 1998. Persistent water level changes in a well near parkfield, california, due to local and distant earthquakes, *J. geophys. Res.,* **103,** 869–889.

Rojstaczer, S., Wolf, S. & Michel, R., 1995. Permeability enhancement in the shallow crust as a cause of earthquake-induced hydrological changes, *Nature,* **373,** 237–239.

Sathe, R.V., Padke, A.V., Peshwa, V.V. & Sukhatankar, R.K., 1968. On the development of fissures and cracks in the region around the Koyna nagar earthquake affected, *J. Univ. Poona Sci. Technol.,* **34,** 15–19.

Scholz, C.H., 2002. *The Mechanics of Earthquakes and Faulting,* The Mechanics of Earthquakes and Faulting, by Christopher H. Scholz, pp. 496. ISBN 0521652235. Cambridge, UK: Cambridge University Press, June 2002.

Srinagesh, D. & Rajagopala Sarma, P., 2005. High precision earthquake locations in Koyna-Warna seismic zone reveal depth variation in brittle-ductile transition zone, *Geophys. Res. Lett.,* **32,** L08310, doi:10.1029/2004GL022073.

Stein, R.S., King, G.C.P. & Lin, J., 1992. Change in failure stress on the southern San Andreas fault system caused by the 1992 magnitude = 7.4 Landers earthquake, *Science,* **258,** 1328–1332.

Talwani, P., 1981. *Hydraulic diffusivity and reservoir induced seismicity.* Final Tech. Rep., U.S. Geol. Surv., Reston, Virginia.

Talwani, P., 1997a. Seismotectonics of the Koyna-Warna area, India., *Pure appl. Geophys.,* **150,** 511–550.

Talwani, P., 1997b. On the nature of reservoir-induced seismicity, *Pure appl. Geophys.,* **150,** 473–492.

Talwani, P., 2000. Seismogenic properties of the crust inferred from recent studies of reservoir-induced seismicity—application to Koyna, *Curr. Sci.,* **79,** 1327–1333.

Talwani, P., Kumar Swamy, S.V. & Sawalwade, C.B., 1996. *Koyna revisited: the reevaluation of seismicity data in the Koyna-Warna area, 1963–1995.* Univ. South Carolina Tech. Report, Columbia, South Carolina.

Talwani, P., Cobb, J.S. & Schaeffer, M.F., 1999. In situ measurements of hydraulic properties of a shear zone in northwestern South Carolina, *J. geophys. Res.,* **104,** 14 993–15 004.

Talwani, P., Chen, L. & Gahalaut, K., 2007. Seismogenic permeability, k_s, *J. geophys. Res.,* **112,** B07309, doi:10.1029/2006JB004665.

Tokunaga, T., 1999. Modeling of earthquake-induced hydrological changes and possible permeability enhancement due to the 17 January 1995 Kobe Earthquake, Japan, *J. Hydrol.,* **223,** 221–229.

Verma, R., 1985. *Gravity field, seismicity and tectonics of the Indian Peninsula and the Himalaya,* Allied Publishers, India.

Walsh, J.B., 1965. The Effect of Cracks in Rocks on Poisson's Ratio, *J. geophys. Res.,* **70,** 5249–5257.

Ziv, A. & Rubin, A.M., 2000. Static stress transfer and earthquake triggering: No lower threshold in sight? *J. geophys. Res.,* **105,** 13 631–13 642.

APPENDIX A: CHARACTERISTICS OF THE RELOCATED EVENTS USED IN THE MODELLING

The characteristics of the relocated events are provided in Table A1 for the events up to the major event of 1967 December 10 and in Table A2 for the events after this date.

APPENDIX B: MODELLING OF THE LAKE BATHYMETRY

Let us consider a point (x_i, y_j) of the reservoir. $d_{i,j}$ is the depth of the bottom of the reservoir at (x_i, y_j). To derive a plausible bathymetry of the lake consistent with the known volume of the reservoir and the known largest depth we adopt the following rules:

(1) (x_{i_o}, y_{j_o}) is the location of the deepest point of the reservoir. It is situated in the neighbourhood of the dam fundations.

(2) The main river flows approximatively from the north to the south following the gradient of the river stream (given by a coefficient γ in m km^{-1}). This provides us with the local depth $d_j^{(r)}$ of the river bed (the superscript '(r)' refers to the river and the subscript 'j' to the NS direction). We assume that the river bed is situated at the most distant point $\zeta_j^{(r)}$ of the lakeshore (excepted in the neighbourhood of the dam). d_{ij} is expected to depend on the distance to the lakeshore ζ_{ij} according to a simple power law $d_{ij} = d_j^{(r)} \cdot [[\zeta_{ij}][\zeta_j^{(r)}]^{-1}]^{\beta}$ with the exponent β which is to be determined.

$d_j^{(r)}$,$\zeta_j^{(r)}$ and ζ_{ij} are known everywhere. To get d_{ij} we need simply to find the exponent β such that the volume of the reservoir in our discretized model is equal to the known volume or in other words:

$\Sigma_{ij} d_{ij} \times S_{xy}$ = Koyna reservoir volume,

where S_{xy} is area of the surface of the rectangular mesh of discretization.

Table A1. Epicentral characteristics and magnitude of events up to 1967 December 10.

Year	Month	Day	Lat.	Lon.	Mag.	Year	Month	Day	Lat.	Lon.	Mag.
1964	10	28	17.65	73.86	3.50	1967	3	13	17.41	73.75	3.10
1964	10	28	17.65	73.86	3.30	1967	4	30	17.35	73.75	3.00
1964	11	3	17.40	73.78	3.40	1967	4	30	17.35	73.75	3.00
1964	11	4	17.42	73.76	3.40	1967	4	30	17.41	73.72	2.90
1965	8	9	17.42	73.76	3.10	1967	6	30	17.41	73.78	3.30
1965	9	12	17.40	73.75	2.80	1967	9	12	17.35	73.78	3.00
1965	11	6	17.42	73.76	3.80	1967	9	12	17.43	73.80	3.20
1965	11	7	17.41	73.79	3.00	1967	9	13	17.35	73.78	3.10
1965	11	8	17.41	73.84	2.90	1967	9	13	17.41	73.82	3.20
1965	11	8	17.36	73.78	3.00	1967	9	13	17.44	73.87	3.20
1965	11	8	17.41	73.84	3.00	1967	10	7	17.57	73.93	2.80
1965	11	8	17.41	73.86	3.60	1967	10	24	17.60	73.82	2.90
1965	11	9	17.41	73.80	3.10	1967	11	4	17.39	73.78	3.30
1965	11	9	17.49	73.88	3.80	1967	11	8	17.41	73.77	3.20
1965	12	27	17.32	73.85	2.60	1967	11	9	17.41	73.75	2.80
1966	1	4	17.32	73.78	3.60	1967	11	18	17.41	73.75	2.70
1966	2	12	17.41	73.84	2.60	1967	11	21	17.40	73.75	3.20
1966	2	24	17.41	73.82	2.00	1967	11	21	17.40	73.75	3.20
1966	6	14	17.30	73.86	3.90	1967	12	1	17.41	73.78	3.10
1966	9	24	17.41	73.75	3.00	1967	12	1	17.41	73.77	3.10
1966	9	24	17.35	73.81	3.10	1967	12	1	17.35	73.80	3.00
1966	9	30	17.41	73.85	3.20	1967	12	2	17.41	73.75	2.10
1966	9	30	17.35	73.82	3.30	1967	12	8	17.37	73.80	3.10
1966	10	5	17.36	73.82	3.10	1967	12	9	17.34	73.81	2.80
1966	10	17	17.41	73.75	2.40	1967	12	9	17.34	73.79	2.40
1966	10	22	17.41	73.75	2.60	1967	12	9	17.29	73.76	2.80
1967	1	14	17.43	73.76	3.10	1967	12	9	17.36	73.82	3.20
1967	1	14	17.44	73.77	3.20	1967	12	9	17.41	73.75	3.00
1967	1	18	17.42	73.75	3.20	1967	12	10	17.38	73.77	3.80
1967	1	18	17.43	73.79	2.80	1967	12	10	17.32	73.79	3.20
1967	1	23	17.39	73.75	3.10	1967	12	10	17.38	73.72	3.60
1967	3	9	17.41	73.75	3.10	1967	12	10	17.35	73.75	6.30

Table A2. Epicentral characteristics of events after 1967 December 10.

Year	Month	Day	Lat.	Lon.	Mag.	Year	Month	Day	Lat.	Lon.	Mag.
1967	12	12	17.23	73.76	4.70	1968	1	3	17.35	73.74	4.00
1967	12	13	17.27	73.88	4.60	1968	1	12	17.41	73.77	4.10
1967	12	13	17.41	73.93	4.60	1968	1	16	17.30	73.82	4.00
1967	12	14	17.31	73.78	4.10	1968	2	7	17.29	73.73	4.30
1967	12	14	17.29	73.80	4.10	1968	2	9	17.25	73.80	4.20
1967	12	14	17.27	73.77	4.00	1968	3	4	17.29	73.81	4.20
1967	12	24	17.28	73.75	4.00	1968	8	31	17.39	73.69	4.10
1967	12	24	17.21	73.58	4.00	1968	9	20	17.41	73.77	4.20
1967	12	24	17.20	73.81	5.00	1968	10	29	17.37	73.75	5.20
1967	12	25	17.23	73.80	4.20	1968	12	5	17.24	73.63	4.30
1967	12	25	17.25	73.75	4.20	1969	2	13	17.38	73.68	4.30
1967	12	25	17.33	73.73	4.60	1969	3	7	17.28	73.73	4.70
1967	12	25	17.29	73.78	4.10	1969	6	27	17.37	73.79	4.70